Advanced optimisation of a mechanical product for its additive manufacturing

Myriam Orquéra, Fabien Albrand, Cristiam Lasso, Dominique Millet, Sébastien Campocasso

Advanced optimisation of a mechanical product for its additive manufacturing

Myriam Orquéra*, Fabien Albrand, Cristiam Lasso, Dominique Millet, Sébastien Campocasso

Université de Toulon, COSMER, Toulon, France

* Corresponding author. Tel.: +33-483-166-613; fax: +33-483-166-601. *E-mail address:* orquera@univ-tln.fr; ORCID: 0000-0001-8339-5041

Abstract

The main objectives of optimising a mechanical system are to reduce costs and increase performance. Thanks to additive manufacturing, it is possible to exploit shape optimisation to place the material where it is needed. This optimisation implies a gain in material and mass but also changes in mechanical behaviour, for example in the connections. Thus, the boundary conditions on the functional surfaces are different before and after the topological optimisation. The objective of this paper is to show that following a topological optimisation, the functional surfaces (i.e. the non-design spaces) have to be redesigned and/or adapted. For this purpose, it is proposed to study a mechanism using two approaches. The first is the simple optimisation of a mechanism along different optimisation paths. The second approach consists in optimising while considering the inter-linkage efforts. The proposed methodology will be applied on a case study which will demonstrate the impact on the performance with an improvement of the functional surfaces. The result of the study shows that by adapting these non-design spaces, the mechanical strength of the parts is improved with the same gain in mass.

Research paper

Keywords: DfAM; Additive manufacturing; mechanical system design; optimisation

1. Introduction

1.1. Study context

Additive manufacturing (AM) processes are now used in the industrial world in the same way as traditional processes. The main advantages of AM are the possibility of making very complex shapes, of adding functions, of obtaining lightweight and near net shape parts. This has opened the field to applications in various sectors such as construction [1], automotive [2,3] or aeronautics [4,5]. The evolution of metal additive

manufacturing [6] processes and the maturity of materials [5] make the use of this technology credible.
In each of these sectors, material and mass savings are generally sought. In this context, it is very common to exploit topological optimisation [7,8], which allows to obtain from a volume, the optimal distribution of material that meets an objective under constraints.
In a mechanical system, which has moving parts that are linked together, topological optimisation affects the mechanical behaviour. The authors [9] have shown previously that the optimisation paths of a so-called open kinematic system has an impact on the computation time, the mechanical behaviour as well as on the mass reduction. In this study, only the design spaces were optimised. However, the topological optimisation also influences the linkage forces and thus the non-design spaces may be also optimised. The focus of this paper is the optimised redesign of a mechanism consisting of linked metal parts.

1.2. Literature

Design for additive manufacturing (DfAM) gathers the method for designing and optimising parts and products while taking into account the constraints of the manufacturing process, exploiting the possibilities of additive manufacturing to improve performance, quality, and cost effectiveness [10].
This definition shows the complexity of the design, which is why many DfAM methodologies have been proposed in the literature.
[11] have distinguished two families of DfAM:

- DfAM in the strict sense which takes into account:
  - AM resign rules,
  - the exploitation of the design freedom offered by AM.
- DfAM in the broad sense which takes into account:
  - the choice of the AM process and the production strategy,
  - the choice of parts to be additively manufactured,
  - manufacturing settings such as machine parameters, hybrid manufacturing (combination of AM and traditional processes), choice of orientation...

Following this analysis, a global design methodology (inspired by the standardised product development and design process VDI 2221) has been proposed to guide novice or experienced designers.
[12] have shown that the skills and knowledges required for AM part design are very extensive.
[13] has proposed a DfAM methodology to gather most of the knowledge needed to design both a part and a mechanism by AM. In this methodology, three families of optimisation have been highlighted:

1. Architectural optimisation, in which the location of the links (between rigid body) must be optimised without manufacturing constraints;
2. Functional optimisation, in which the potential of the AM is exploited;
3. Topological optimisation (supplemented by parametric optimisation if necessary).

In the paper [9], a method for the optimisation of a complex, open-chain mechanical system was proposed. This method - which is called Topological Optimisation of a Mechanical System (TOMS) - performs Topological Optimisation Loops (TOL) taking into account changes in boundary conditions (Fig. 1). The boundary conditions change as the mass (or inertia) of the components decreases due to their topological optimisation.

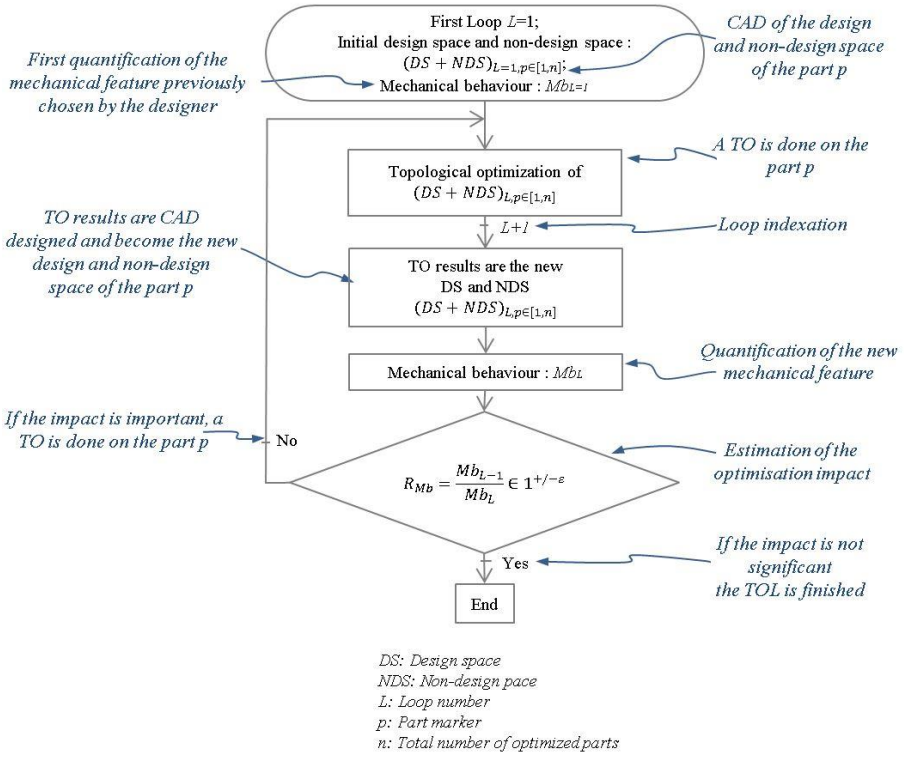

Fig. 1. Topological optimisation loop (TOL) organization chart considering inertia and mass decrease [9]

These methodologies perform the optimisation of design spaces and do not include the optimisation of non-design spaces.

The design space (DS) is the volume that can be modified during an optimisation [14,15]. For [16], design space is defined as a volume that is used to connect functional surfaces (FS) and help them fulfil their functional roles. The design space should be as large as possible "to explore all opportunities for design improvement" as advised by [17].

A non-design space (NDS) is the volume of the part in which the software does not change the material distribution. Non-design spaces are:

- used to represent an external part (such as a bush bearing),
- a volume that should not be modified (such as a logo, or a pipe),
- volumes on which functional surfaces are loaded.

The design example for AM proposed by [18] shows first the optimisation of design spaces. A hydraulic connector made by conventional processes is completely redesigned and adapted to AM to improve its performance and mass. Thus, the non-design spaces ensuring fluid guidance or the embedding links with external parts have been optimised among others to decrease the drop pressure.
[19] has proposed a topological optimisation of a part in which the number and the positions of the embedded links are variables of the topological optimisation.
Generative design is an additional tool that allows a multitude of topological optimisation (TO) results to be obtained according to multiple criteria (price, mechanical strength, manufacturing process, etc.). [20] shows the potential of this tool and proposes a method for optimising a part.

These methodological proposals make it possible, for a single part and in a static case, either to take into account the constraints of the technological solutions, or to obtain the best positioning and number of inserts. However, the non-design spaces are not modified after the topological optimisation, even if the boundary conditions applied to these volumes are no longer the same.

1.3. Article scope

Thus, most of the time non-design spaces are designed at the first design and sized to meet mechanical stresses as well as constructive constraints (operating and / or technological solution). This state of the art highlights the lack of adaptation of NDS when setting up optimisation loops as shown in the Fig. 2. The objective of this article is to propose the application of a method for designing a complex system by exploiting topological optimisation loops (TOL).

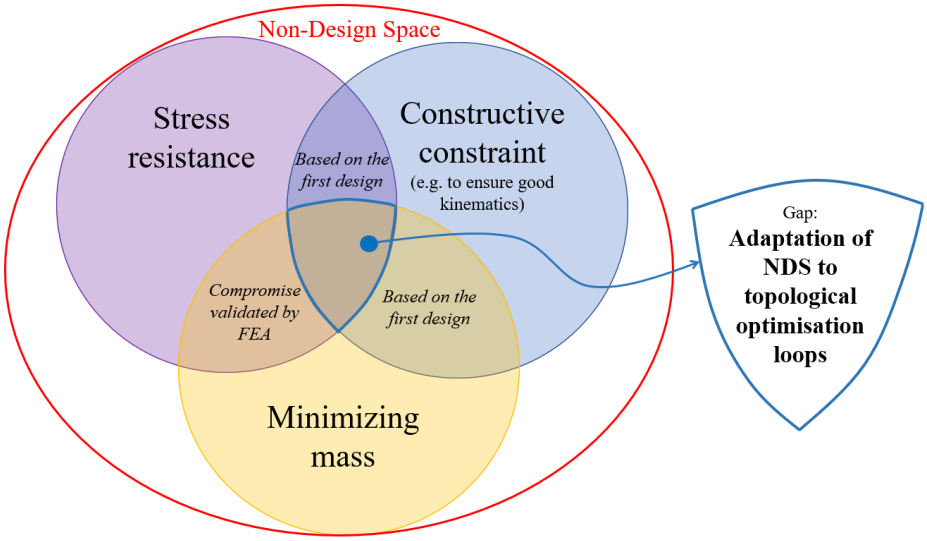

Fig. 2. Non-Design Space (NDS) requirements achieved to date and shortcomings (colour figure online)

To achieve this objective, the remainder of this manuscript is divided into three parts. The first will detail the method used by the authors. The second is the setting up of the case study. Finally, the article will end with the conclusion and perspectives.
The chapter on the study case will start with the presentation of the mechanism studied. This is followed by the presentation of the methodology. Then, different optimisation paths are explored, to choose the path performing the best mass gain due to the topological optimisation of the parts. Afterwards, it is shown how the non-design spaces are redesigned. Therefore, an optimisation loop to consider these new non-design spaces is performed and validated by finite element analysis. A discussion of the findings concludes the case study.
This article will end with a conclusion on the contributions of this methodological approach.

2. Research method

In order to show, on the one hand, the importance of taking into account the results of TO in the behaviour of functional surfaces, and on the other hand how to apply the redesign, two approaches are proposed.

- A first study consists in applying the TOMS method following the three paths proposed in [9]. The results will be compared to this article to complete the criteria for choosing a path. Following the results of this study, the optimisation path with the most interesting results will be selected for the implementation of a design methodology, which is the subject of the second study (Fig. 3).
- The second study demonstrates the application of a methodology to achieve optimisation for the non-design space. This research strategy is summarised in the diagram in Fig. 4. The methodology is implemented to optimise not only the design spaces but also the non-design spaces throughout the topological optimisation.

The results of this second study will be compared to the first one in order to highlight the interests.

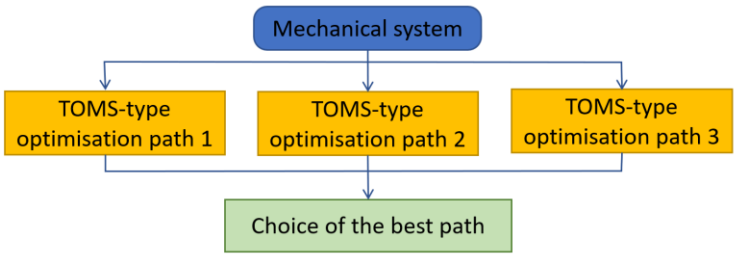

Fig. 3. Research strategy for the first study (colour figure online)

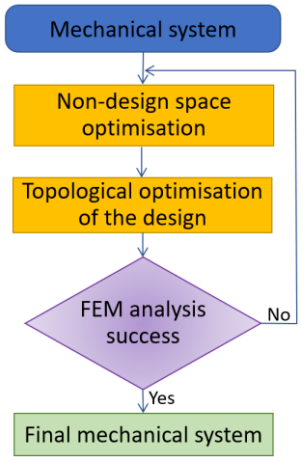

Fig. 4. Framework to optimise both space design and non-design space (colour figure online)

Both studies are carried out on the same case study, the results of which will be analyzed and compared to the original product.

3. Case study

3.1. Case study presentation

3.1.1. Four-stroke diesel engine

The case study is a single-cylinder 4-stroke diesel engine (Fig. 5). This type of engine is used as the basis for analyses of multi-cylinder engines [21].

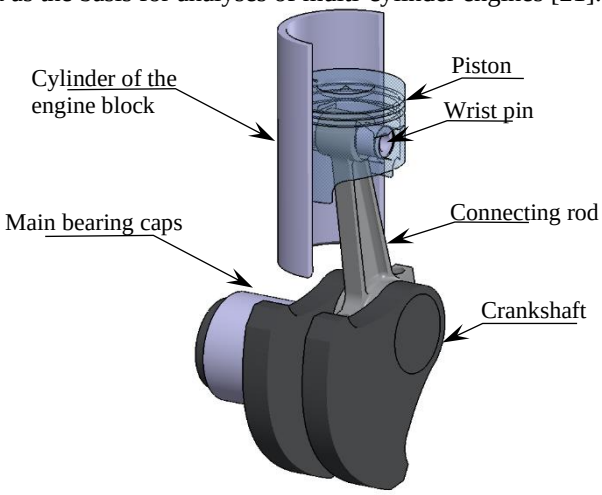

Fig. 5. Presentation of the study case, single-cylinder 4-stroke diesel engine (colour figure online)

3.1.2. Assumptions and restrictions of the study

To simplify the approach, the study will not deal with thermal stresses due to fuel ignition and heat removal.
The piston, connecting rod and crankshaft will be studied in the optimisation paths. It is evident that all parts that interact with the optimised components will have to be redesigned afterwards, e.g. the crankcase. This will not be discussed in this article.
The friction between the parts is neglected, as well as the effects of gravity in comparison with the intensity of the forces involved.
The following dimensions will remain fixed throughout the study: the connecting rod centre-to-centre distance, the stroke and the piston diameter.

The non-variable data of the study are :

Piston diameter: d=70 mm
Stroke: c=72 mm
Connecting rod centre-to-centre distance: L=130 mm
Ignition pressure: P=100 bar
Crankshaft speed: ω=4500 rpm

The pressure of 100 bar is the relative pressure to atmospheric pressure at full load for the given diesel engine speed ω=4500 rpm.

3.1.3. Materials

The parts studied are optimised for additive manufacturing using the laser powder bed fusion (L-PBF) process. For this reason, the finite element analysis study of the original parts is carried out with materials adapted to this process. This perfoms the mechanical behaviour of the parts to be determined and compared with the behaviour of the optimised parts.
The piston is made of 316L [22] and the connecting rod of TiAl6V [23]. The crankshaft will continue to be a part made by traditional processes (forging or casting) and then machined in 42CrMo4.

Initial part	**Material**	**Young modulus E (Gpa)**	**Density ρ (g/cm3)**	**Yield strength Re (Mpa)**	**Mass (g)**
Piston	316L	182	7,95	491	687
Connecting Rod	TiAl6V	131,5	4,5	1110	253
Crankshaft	42CrMo4	210	7,85	730	4295

Table 1. Summary of materials suitable for AM and characteristics of original parts

3.2. Method

The detailed steps of the method used in this case study are shown in the flowchart in Fig. 6.

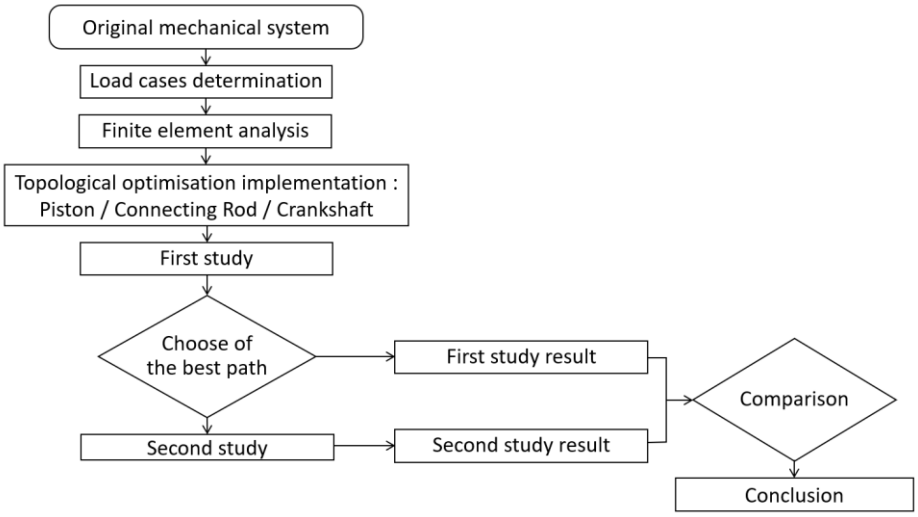

Fig. 6. Workflow of the study.

3.2.1. Load cases

The loading of the piston and connecting rod is studied for all four strokes. The choice of load cases -for topological optimisation- is defined by studying the forces undergone by each rigid body for each stroke. The maximum intensity will be taken into account as shown in Fig. 7 for the piston and in Fig. 8 for the connecting rod.

The piston is subjected to the forces of the connecting rod (Fb), the gas (Fg) and the cylinder (Ft). Fig. 7 shows the evolution of these forces as a function of the crankshaft angle (α). The piston will be optimised under the five load cases detailed in Fig. 7.

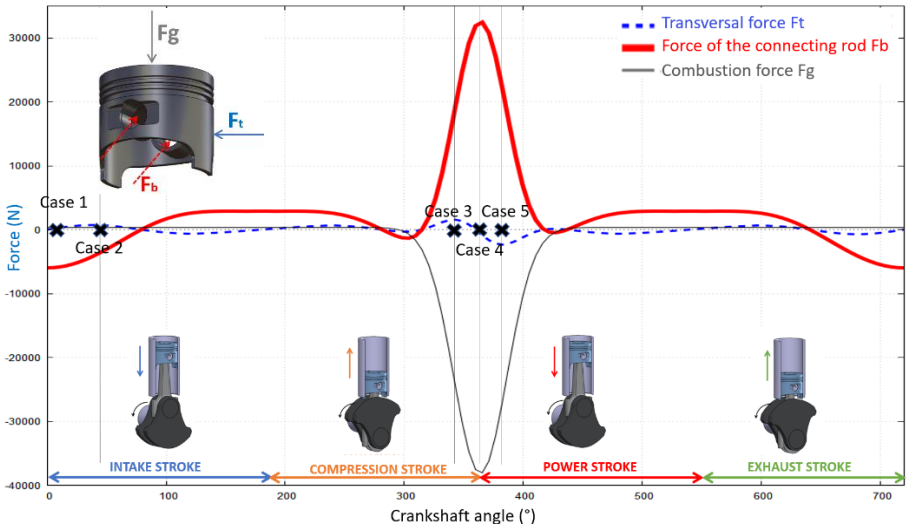

Fig. 7. Load curves for the piston and choice of load cases (colour figure online)

The different load cases of the piston were chosen as follows:

- Case 1: Force exerted at the beginning of the cycle when the piston is at top dead centre,
- Case 2: Maximum transverse force and opposite to the force exerted by the connecting rod,
- Case 3: Maximum transverse force over the entire operating cycle,
- Case 4: Maximum gas force over the entire duty cycle,
- Case 5: Transverse force in addition to the gas forces and opposing the force exerted by the connecting rod.

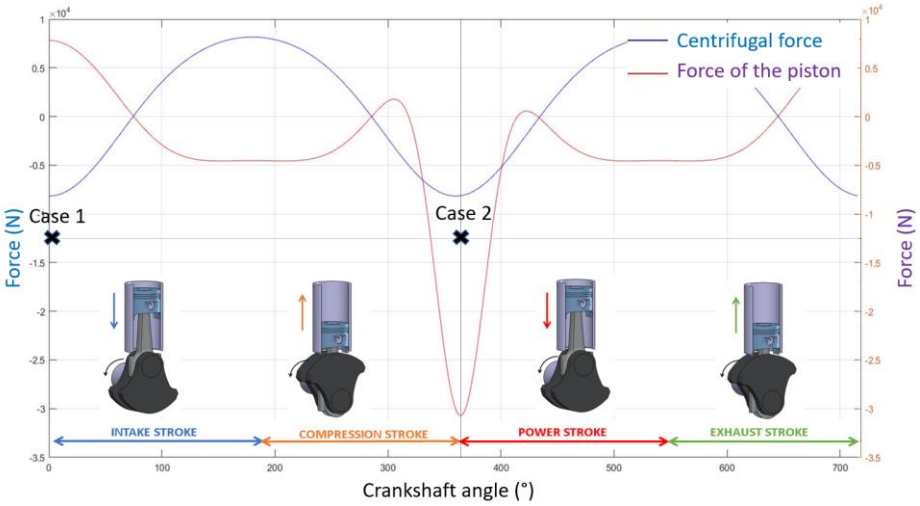

Fig. 8. Load curves for the connecting rod and choice of load cases (colour figure online)

The different load cases of the connecting rod were chosen as follows:

- Case 1: Maximum tensile force on the connecting rod during intake. The connecting rod is subjected to traction due to the inertia of the piston,
- Case 2: Maximum compression force on the connecting rod during ignition.

3.2.2. Behaviour of original parts

The finite element study of the mechanical behaviour was carried out on the piston. The boundaries conditions are detailed in the Fig. 12. The five load cases were imposed. The maximum stress obtained is 220 MPa for the fourth load case. The safety coefficient is equal to 2.2 (as shows the Fig. 9).

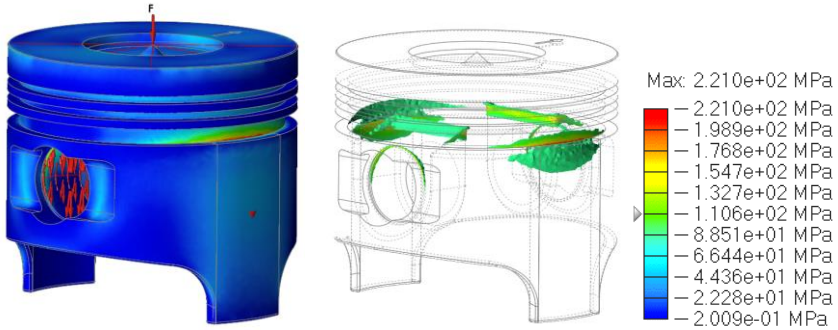

(a) (b)

Fig. 9 Stress distribution in the piston (a); Highlighting of internal stresses (b) (colour figure online)

The finite element study of the mechanical behaviour was carried out on the connecting rod (Fig. 8) for the two load cases. The results show that in case 1, one obtains the highest equivalent Von Mises stress which is equal to 369 MPa. This is equivalent to a minimum safety factor of 3 (Fig. 10).

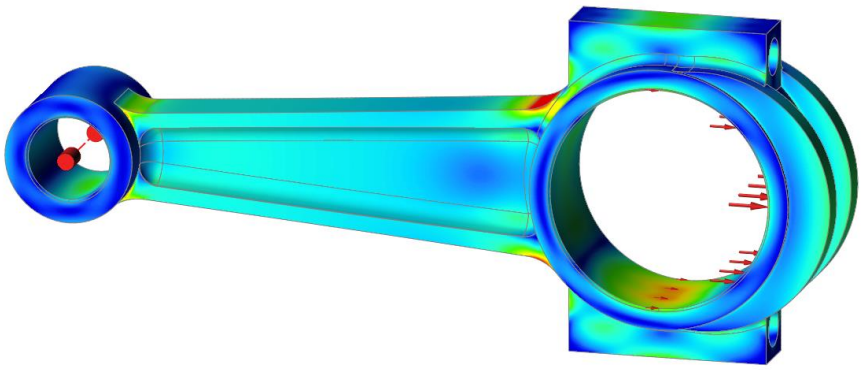

Fig. 10 Stress distribution in the connecting rod (colour figure online)

3.2.3. Implementation of optimisations

Design spaces are shown in green and non-design spaces in orange in Fig. 11. These spaces fill the free volume as much as possible while allowing the movements of the linked parts.

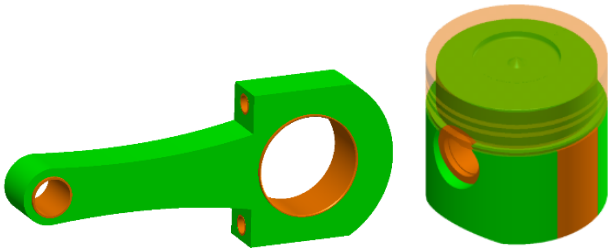

Fig. 11 Definition of design (green) and non-design (orange) spaces for the connecting rod (left) and piston (right) (colour figure online)

As for the boundary conditions, the connecting rod small-end bearing is embedded, and the rotating big-end bearing will be loaded. Two planes of symmetry are imposed on the design space (Fig. 12 (a)).
For the piston (Fig. 12 (b) and (c)), the piston crown will be subjected to the gas forces, and the wrist pin hole to the inertia, connecting rod, and transverse forces. The skirt will be considered fixed. A plane of symmetry is imposed on the design space.

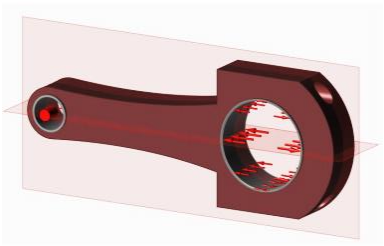

(a)

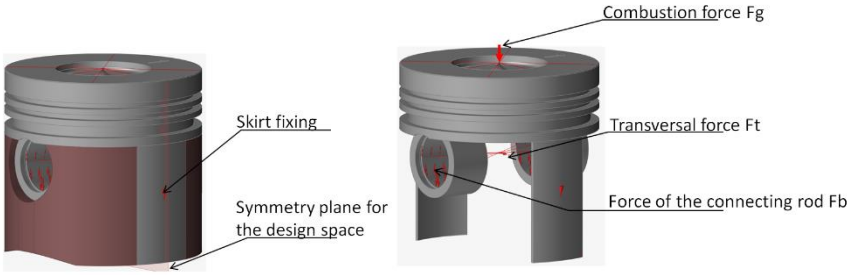

(b) (c)

Fig. 12 Boundary conditions and planes of symmetry for the connecting rod (a) and piston (b) and (c) (colour figure online)

The parts (piston and connecting rod) are optimised, following different paths, until convergence is reached. The convergence is based on a mechanical criterion [24]. In this study, we want to decrease the masses and inertias of the moving components in order to reduce the bouncing and longitudinal (first order) vibration nuisance (Fig. 13).

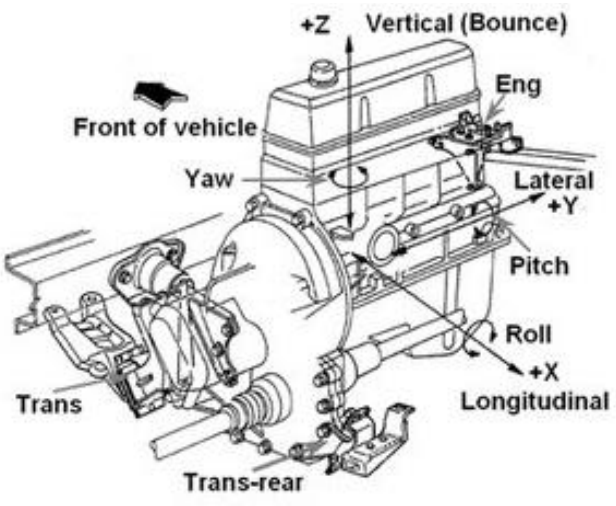

Fig. 13. Powertrain movements [25]

Only the rotating mass influences the longitudinal vibration (Equation 1 and Equation 2). Alternating and rotating masses influence the bounce (Equation 3 and Equation 4) [21,26].

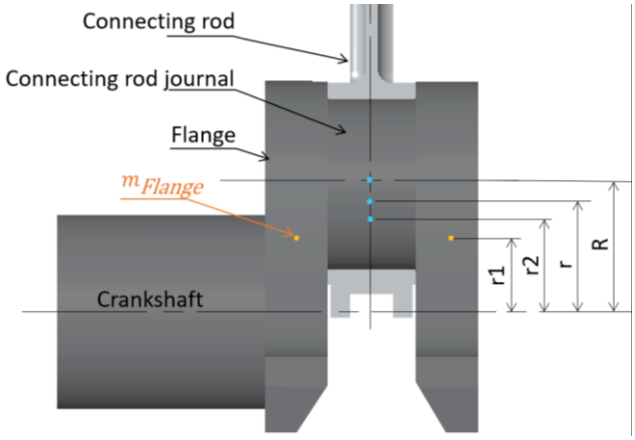

Fig. 14. Settings to estimate loads (colour figure online)

Equation 1

$$F_{LV} = -M_{rotf}.R.\omega^2.\sin(\alpha)$$

Equation 2

$$M_{rotf} = 2.m_{Flange}.\frac{r1}{R} + m_{ConnectingRodJournal} + \frac{2}{3}.m_{ConnectingRod}$$

Equation 3

$$F_{Bounce} = (M_{Alt} + M_{rotf}).R.\omega^2.\cos(\alpha)$$

Equation 4

$$M_{alt} = m_{piston} + \frac{1}{3}.m_{ConnectingRod}$$

With (parameters are shown in Fig. 14)

F_{LV} : Longitudinal vibration force
M_{rotf} : Rotating mass to estimate the force
ω : Crankshaft rotational speed
α : Angular position of the crankshaft
R : Half stroke
m_i : mass oh the part *i*

Thus the convergence of the optimisations (Equation 5) of the connecting rod will be done on the longitudinal vibration ($Mb_L = F_{LV}$) and that of the piston will be done on the bounce ($Mb_L = F_{Bounce}$) [9].

Equation 5

$$R_{Mb} = \frac{Mb_L}{Mb_{L+1}} \in 1^{+/-\varepsilon} \text{ with } \varepsilon = 0.1$$

Therefore, the objectives of optimisation can be established as follows:

- For the piston: Maximize stiffness with a constraint of 35% of the mass,
- For the connecting rod: Maximize stiffness and frequency with a constraint on the mass (which will be detailed in each case).

The crankshaft must make it possible to balance the single-cylinder. For this, it must be sized to balance the rotating mass and the alternative mass.
The balancing of the rotating mass is done with the help of the counterweight. Thus, each counterweight must meet Equation 6.

Equation 6

$$M_{Counterweight\_ROT} = \frac{R}{2.y_1}.M_{rotf}$$

With

y_1 : center of gravity of the counterweight,
$M_{Counterweight\_ROT}$: Mass of the counterweight
M_{rotf} : defined in Equation 2

The position of the center of gravity of the counterweight y_1 is established according to the free volume and must be as large as possible to decrease $M_{Counterweight\_ROT}$.

Balancing bounce movements of order 1 can be achieved by several methods:

- Setting up two primary balancing shafts,
- Setting up one primary balancing shaft,
- Setting up no primary balancing shafts (the first order of the bouncing vibration effort is balancing and there appears a longitudinal vibration effort of order 1).

In this study it will be retained the latter case. The crankshaft will receive the mass detailed in Equation 7 which will be added to each counterweight mass $M_{Counterweight\_ROT}$.

Equation 7

$$M_{Counterweight\_ALT} = \frac{M_{alt}}{2}$$

To optimise the crankshaft while respecting these data, it will be imposed the mass $M_{Counterweight\_ROT}$ which is indicated in orange in Fig. 15. A design space (in green in Fig. 15) will be subjected to topological optimisation with a stiffness objective and a constraint on the mass such that the percentage meets Equation 8.

Equation 8

$$MassConstraint\% = \frac{M_{Counterweight\_ALT}}{M_{Design\_Space}}.100$$

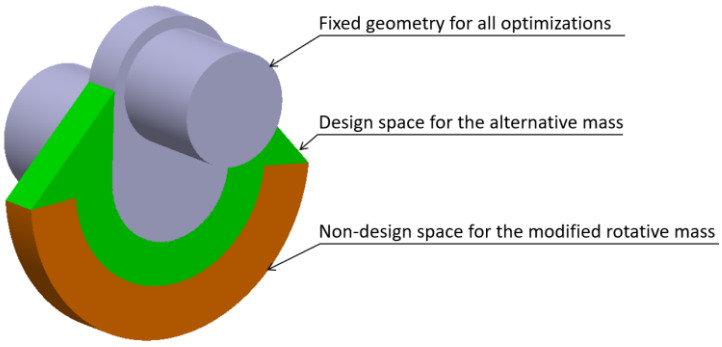

Fig. 15. Crankshaft section for optimisation. Design spaces for the alternative mass (in green), the orange part is the rotating balancing mass, the gray parts are the frozen elements during the study (colour figure online)

The optimisation of the crankshaft must consider the traditional manufacturing process (molding or forging and machining). Therefore, topological optimisations will be

subject to manufacturing constraints. For this the optimisation model will be subjected to the extrusion constraint as shown in Fig. 16 (a). The crankshaft bearing is embedded, and the rotating counterweight undergoes a radial centrifugal force detailed in Equation 9.

Equation 9

$$F_{centrifugal} = M_{Counterweight\_ROT}.\omega^2.R$$

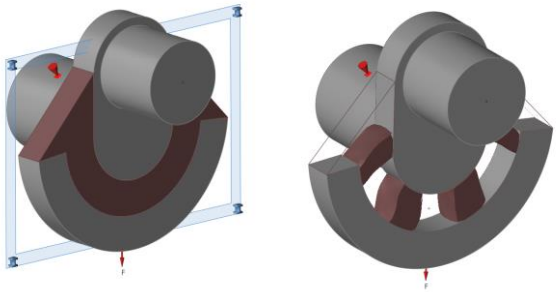

(a) (b)

Fig. 16. (a) Manufacturing constraints - of the extrusion constraint type - imposed during the topological optimisation of the alternative mass. (b) Results of topological optimisation (colour figure online)

The extrusion constraint leads to obtain a geometry that can be easily machined (Fig. 16 (b)) and whose mass of the design space obtained approaches the target alternative mass.

For each optimisation, the mechanical strength of each part is checked by finite element analysis to ensure a safety coefficient greater than or equal to 1.5.

3.3. First study: Optimisation following the three paths

In order to best show the progression of the study without repetition, only the first path will be detailed and the results of the two others will be directly provided

3.3.1. Path 1: Piston then connecting rod

The piston is optimised according to the objectives mentioned above, the results are shown in Fig. 17. The resulting evolution of the bouncing vibration is shown in the Fig. 18.

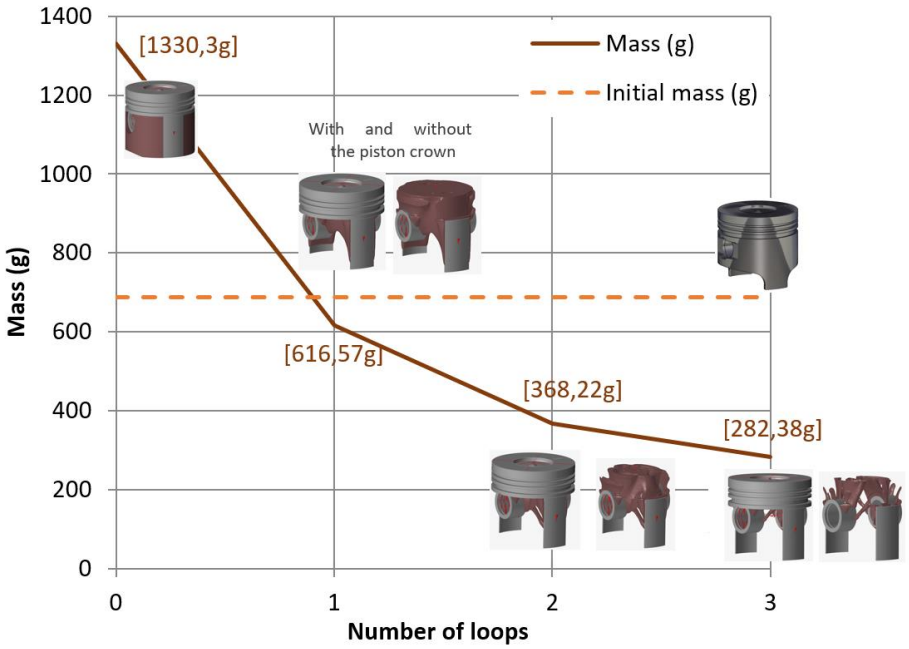

Fig. 17. Evolution of piston mass during optimisations of the path 1 (colour figure online)

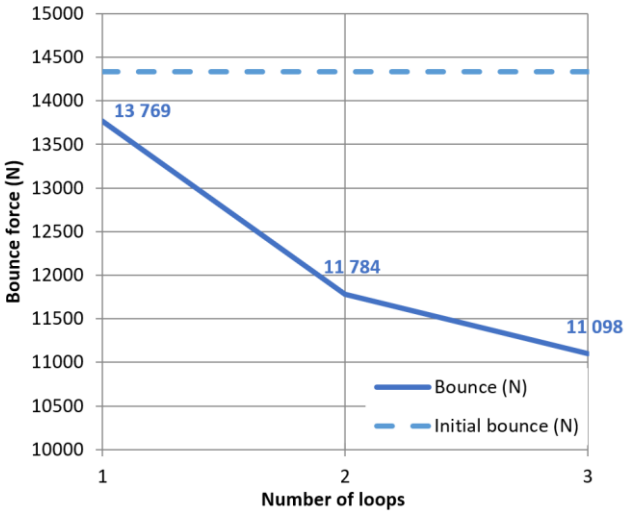

Fig. 18. Influence of optimisation loops on the bouncing vibration (colour figure online)

The objective of connecting rod optimisation is the minimization of compliance and maximizing the eigen frequency with constraint on the mass at 35%.

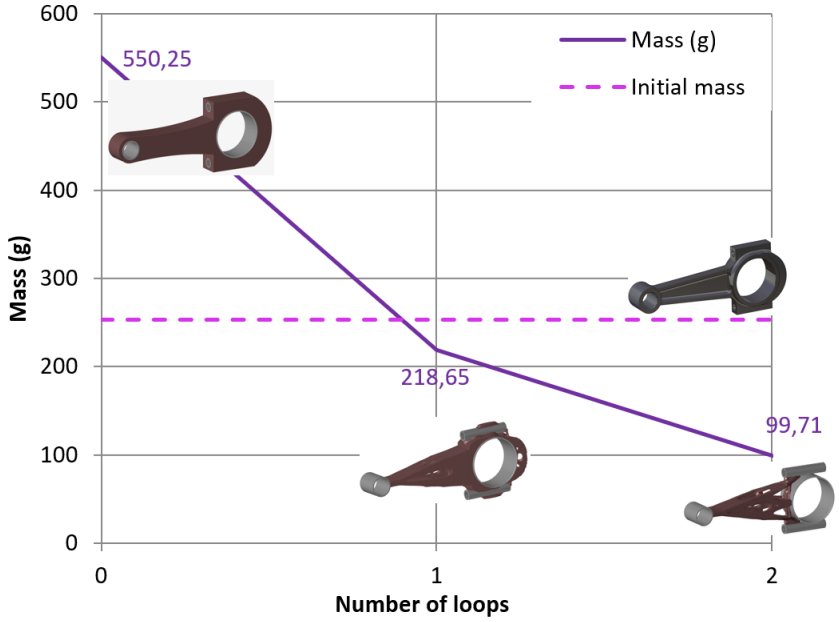

Fig. 19. Evolution of the mass of the connecting rod during the optimisations of path 1 (colour figure online)

The vibration forces at zero iteration are determined by considering the characteristics of the connecting rod with the initial DS and NDS, and the optimised piston (see the Fig. 20).

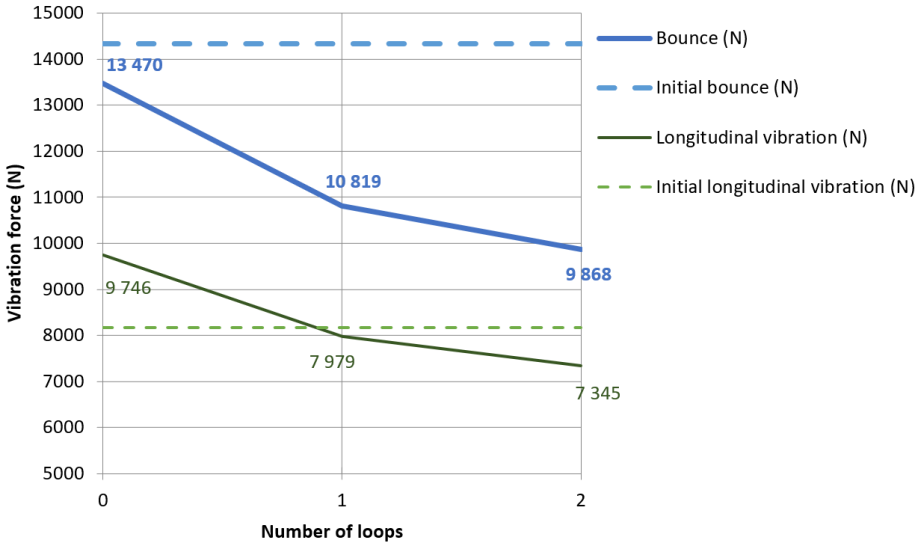

Fig. 20. Influence of optimisations on the bouncing and longitudinal vibrations (colour figure online)

The masses obtained thanks to the topological optimisation of the crankshaft meet the constraints mentioned in the section 3.2.3. The final mass of the crankshaft reaches 2023g for path 1. The result of the optimisation is shown at the Fig. 21.

Fig. 21. Redesign of the crankshaft after optimisation for path 1 (colour figure online)

At the end of these optimisations, a redesign is carried out in order to improve the shapes of the optimised parts (smoothing operation) and to impose rounded edges (Fig. 22). This is done by taking into account the manufacturing constraints of the L-PBF [27,28].

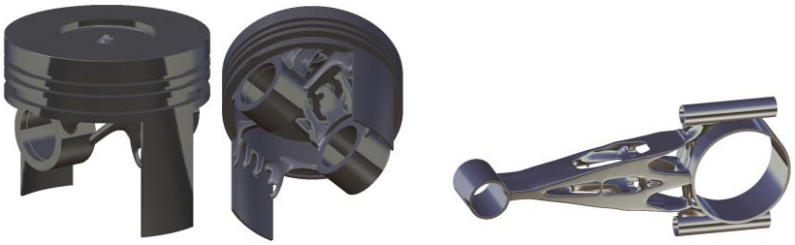

Fig. 22. Redesign of the piston on the left and the connecting rod on the right.

From this reconstruction, a finite element verification is carried out with the same boundary condition of the Fig. 12 and load cases of the Fig. 7. The stress resistance of the piston and connecting rod shows that the safety coefficient is 1.76 for each of them (Fig. 23 and Fig. 24). The forces subjected to the piston and connecting rod are derived from the results of the optimisations.

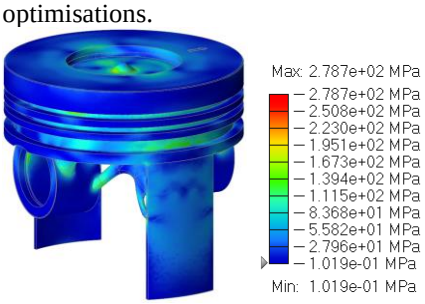

Fig. 23. Von Mises stresses of the re-designed piston (colour figure online)

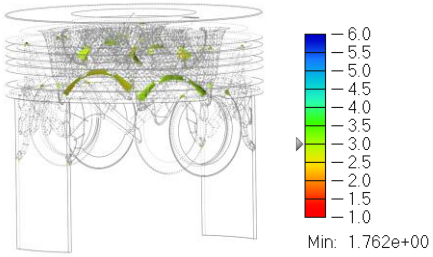

Fig. 24. Safety factor of the re-designed piston (colour figure online)

3.3.2. Results of the first sudy

As previously announced, in order not to be redundant, the studies of path 2 and 3 are not detailed but the results are shown in Table 2.

	Initial system	Path 1 : Piston -> Connecting Rod	Path 2 : Connecting Rod -> Piston	Path 3 : Piston + Connecting Rod
Piston Mass (g)	687	317	318	317
Gain (%)		54	54	54
Connecting Rod Mass (g)	253	113	152	210
Gain (%)		55	40	17
Bounce (N)	14335	9868	10506	10510
Gain (%)		31	27	27
Longitudinal vibration (N)	8165	7345	7768	7772
Gain (%)		10	5	5
Torque (N.m)	171,69	195,25	194,46	193,42
Gain (%)		13,7	13,3	12,7

Table 2: Summary of the results of the 3 paths

The Table 3 summarizes the crankshaft optimisation results as well as the total mass of the "Piston + Connecting Rod + Crankshaft" assembly for each of the paths. The total mass gain on the assembly {piston, connecting rod, crankshaft} reaches 25.7% for path 1.

	Path 1	Path 2	Path 3
$M_{Counterweight\_ROT}$ (g)	484,9	497,7	517,4
$M_{Counterweight\_ALT}$ (g)	177,3	184,3	193,5
MassConstraint% (%)	31,4	33,1	35,8
Centrifugal force (N)	165,9	170,4	176,7
Crankshaft mass (g)	2023,0	2046,3	2066,2
Total mass (g)	2453	2516	2593

(Piston+Connecting Rod+ Crankshaft)			
Total mass gain (%)	25,76	23,84	21,51

Table 3: Summary of crankshaft optimisations for the three paths

The Fig. 25 shows the CAD of the engine for the three paths.

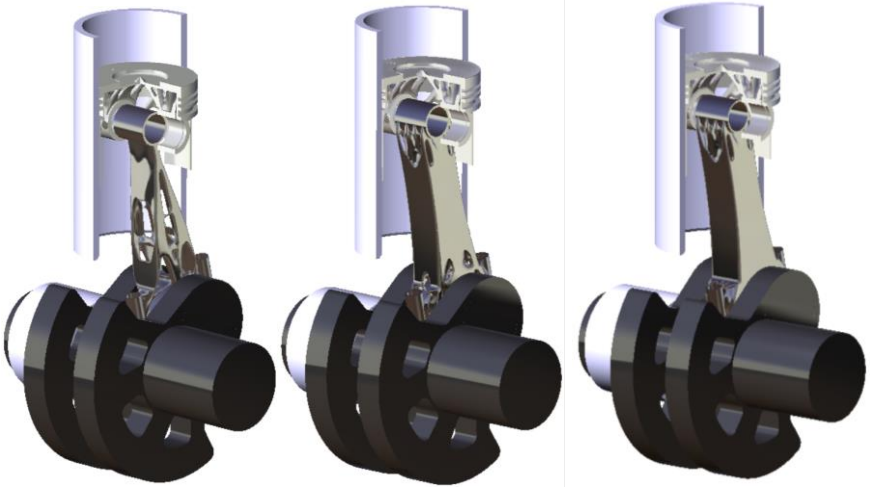

(a) (b) (c)

Fig. 25. CAD of the engine for path 1 (a), path 2 (b), path 3 (c). The piston is in quarter cut. (colour figure online)

3.3.3. Discussion

At the last stage of this study (Fig. 3) the results of each optimisation path are compared. Based on the Table 2 -in which are all the results and gain for each of the paths considering the redesign of the parts- path 1 shows better mass gains for the connecting rod (61%) and also a clear decrease in bouncing vibration (31%) and longitudinal vibration (10%). The mass gain of the piston is almost identical for all three paths.

Engine torque T is determined by the sum of torque due to the effects of the gas T_g and torque due to inertial effects T_i, as shown in the Equation 10. The latter torque is influenced by variations in the alternate mass M_{alt} (Equation 4). Thus the value of the engine torque increases favorably when the alternating mass decreases. The Table 2 indicates that the highest gain is 13.7% for the first path.

Equation 10

$$T = T_g + T_i$$

For all the reasons mentioned above, the rest of the study will focus on path 1.

This choice of path can be made a priori by identifying the part that has the most impact on the objectives of the design. In this case study, it is desired to reduce the vibration forces of the bouncing and longitudinal type as well as to increase the engine torque. The characteristic to have the greatest possible effect on these vibrational forces and engine torque is sought. The study of reduced sensitivity S* [29] will be performed to determine which part has the greatest impact. This makes it possible to compare the effects of coefficients that do not have the same unit. The reduced sensitivity coefficient S* is determined for each characteristic, from each of the formulae given in the Table 4.

Feature *Ci*	m_{piston}	$m_{connecting\_rod}$
$S^*(F_{Bounce}\max/C_i) = C_i.\frac{\partial F_{Bounce}}{\partial C_i}$ (N)	$7.99 \times m_{piston} = 5.49$	$7.99 \times m_{connecting\_rod} = 2$
$S^*(F_{Longitudinal}/C_i) = C_i.\frac{\partial F_{Longitudinal}}{\partial C_i}$ (N)	0	-0.66
$S^*(T/C_i) = C_i.\frac{\partial TMAX}{\partial C_i}$ (N.mm)	For alpha =325° -31.5	For alpha =325° -7.75

Table 4: Influence of characteristics on engine behaviour

It should be noted that the piston has a strong influence on the bouncing vibrations (2.7 times greater than the connecting rod) while only the connecting rod influences the longitudinal vibrations. Finally, the piston influences 4 times more than the connecting rod on the torque.
It can be noted that, most mechanisms have a rigid body by which mechanical energy is transmitted as input or output of the mechanism. Comparing these results with those proposed by [9], it can be noticed that optimising first this rigid body makes it possible to obtain the main gain whether for a closed or open system.

3.4. Second study: Inter-link impact analysis

In this second study, the method presented in the Fig. 4 is used. This method makes it possible to adapt "a priori" the non-design spaces to the estimated gains.

3.4.1. Optimisation of non-design spaces

Engine parts are linked together by functional surfaces or technical components. These surfaces and components must be sized to meet the stresses and constraints of the technological solution. In the Fig. 26, the connections are indicated between the functional surfaces of each part.

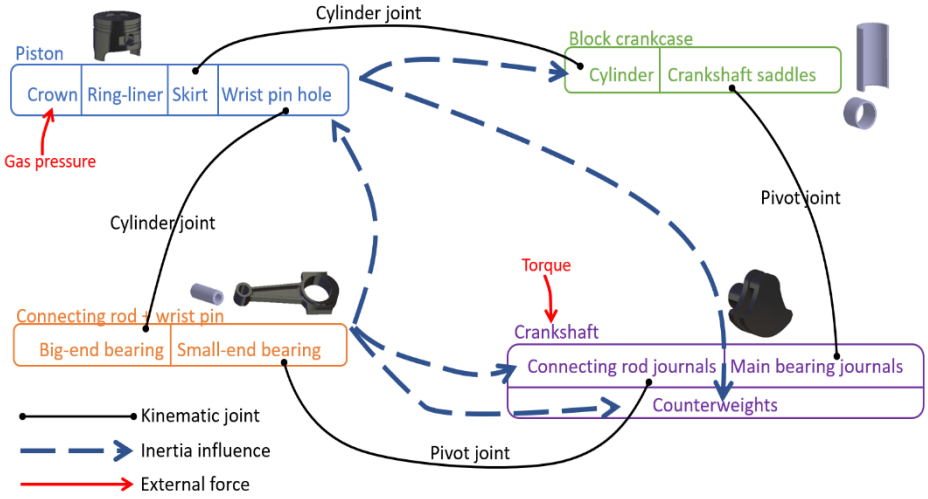

Fig. 26. Graph of the connections of the system {Piston, connecting rod, crankshaft, crankcase} decomposed into functional surfaces, the influences of inertia and external forces (colour figure online)

Optimisations have led to a gain in mass and inertia. The influence of the variation of inertia is indicated between the parts in the Fig. 26.
In general, the decrease in inertia is favorable for mechanical behaviour. However, the inertia of the connecting rod enable to "counter" the gas forces on the piston as shown in the Equation 11. This equation indicates the strength of the connecting rod on the piston following the axis of the connecting rod.

Equation 11

$$F_b = \left(M_{alt}.R.\omega^2.\left[\cos(\alpha) + \frac{\cos(2.\alpha)}{\frac{L}{R}}\right] - F_g \right).\frac{1}{\cos(\beta)}$$

With:

$$\cos(\beta) = \sqrt{1 - \frac{sin^2(\alpha)}{\lambda^2}}$$

Reducing the inertia of the connecting rod thus induces an increase in the forces on the piston. Fig. 27 shows the difference between the initial force of the connecting rod on the piston and that following the optimisation of path 1.

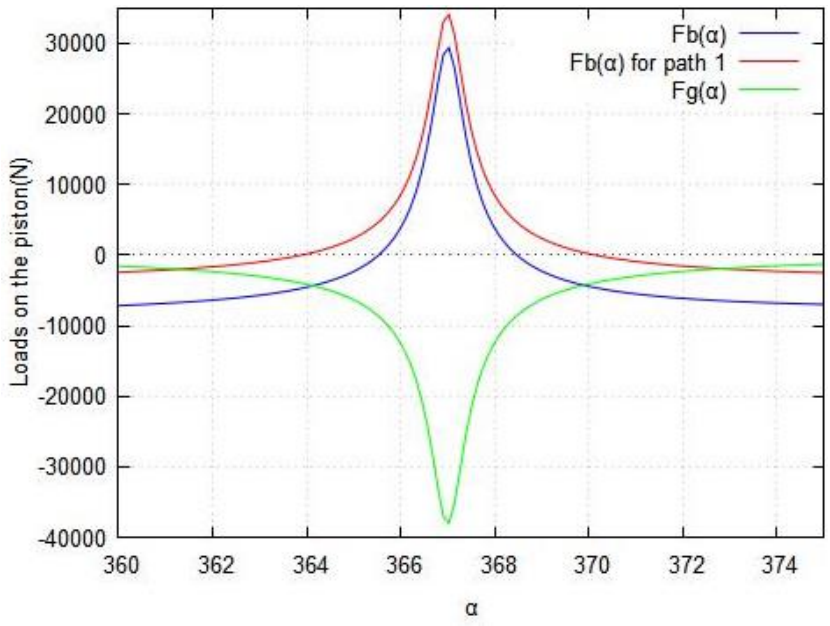

Fig. 27. Highlighting the strength of the connecting rod on the piston before optimisation and then after path 1 (colour figure online)

The curve of the Fig. 28 shows the evolution of the maximum force of the connecting rod on the piston during iterations for path 1.

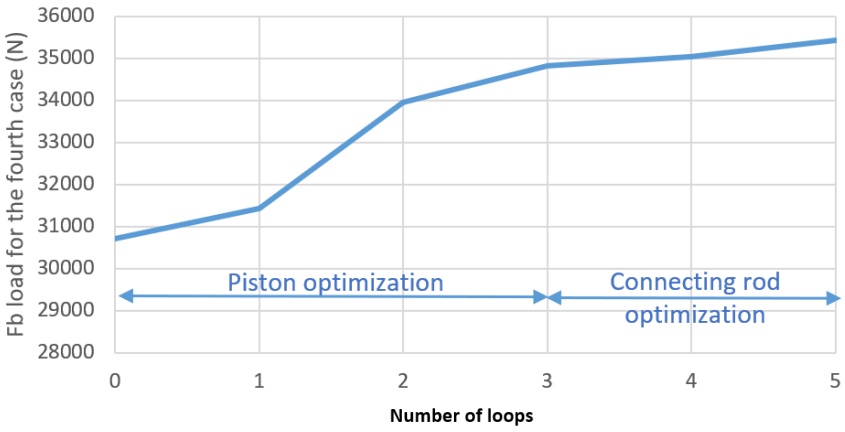

Fig. 28. Evolution of connecting rod forces on the piston during iterations for load case number 4 (combustion stroke) (colour figure online)

These forces are transmitted to the piston via the axis. The dimensioning of the gudgeon pin and the bearings must again be carried out to ensure the good performance of the

link. For this, the diameter of the gudgeon pin has been resized to meet the following constraints [30] :

- shear resistance (Equation 12)
- the maximum longitudinal deformation (Equation 13)
- the maximum pressure for the bearing (Equation 14).

As shown in Table 5, the diameter of the axis (of material 20MnCr5, Re=720Mpa, safety coefficient s=2) which was initially 25.5 is resized to 29 mm to meet all constraints. Equation 12 to Equation 14 express the relationships between the geometric parameters and the forces involved.

	Initial	Path 1
Gudgeon pin diameter D (mm)	25,5	29
Deformation f (µm)	28,9	22,2
Permissible deformation (µm)	30,4	30,4
Shear stress (Mpa)	271,4	273,5
Permissible shear stress (Mpa)	288,0	288,0
Small-end bearing pressure (Mpa)	18,52	18,8

Table 5: Sizing of the piston axis and bearing

Equation 12

$$\tau = \frac{F_b}{\frac{\pi}{2}.(D^2 - d^2)} \leq 0{,}8.\frac{Re}{s}$$

Equation 13

$$f = \frac{0{,}12.F_b.L^3}{E.(D^4 - d^4)} \leq 0{,}4.10^{-3}.D_{piston}$$

Equation 14

$$p = \frac{F_b}{D.L} \leq p_{max}$$

Fig. 29 and Fig. 30 detail the non-design spaces as well as the geometric parameters used for resizing.

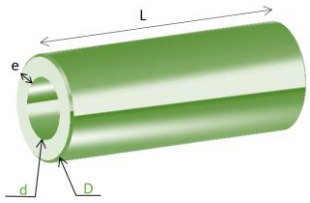

Fig. 29. Geometric parameters of the non-design spaces of the gudgeon pin. Parts and parameter in green are the variables to be optimised. In black, unmodified parameters and spaces.

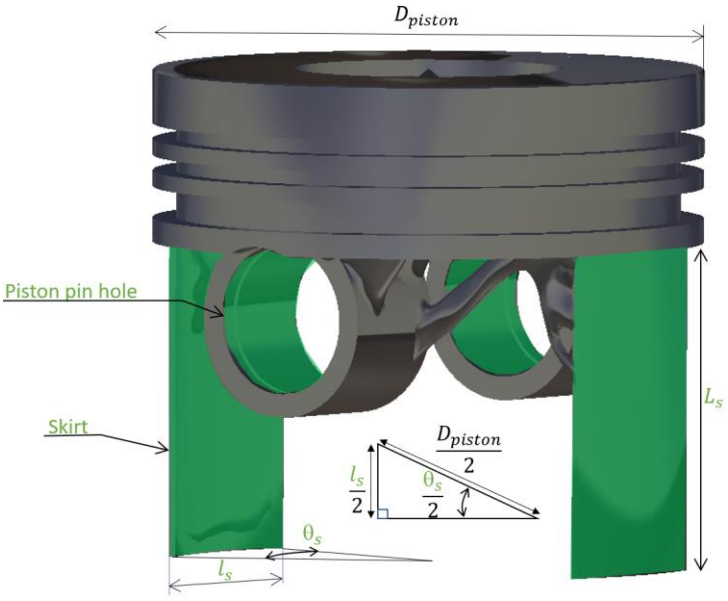

Fig. 30. Geometric parameters of the piston non-design spaces. The parts and parameters in green are the variables to be optimised. In black, unmodified parameters and spaces. (colour figure online)

The transverse forces of the cylinder on the piston are also a function of the alternating mass. When it decreases, the transverse force also decreases (Fig. 31).

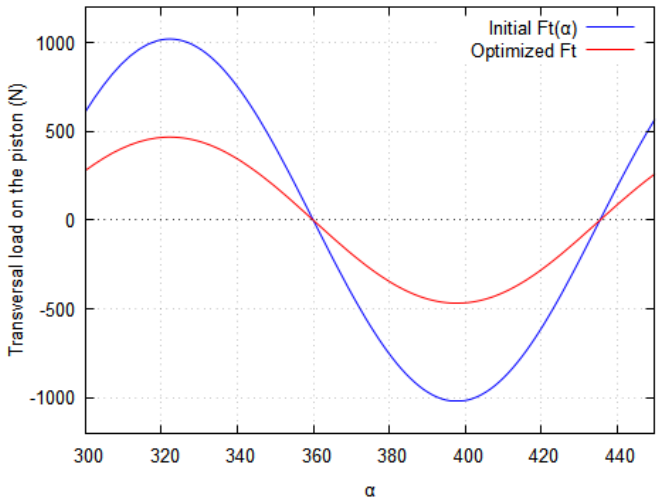

Fig. 31. Evolution of transverse forces on the piston during iterations, in the initial case and for path 1. (colour figure online)

This is why the piston skirt must also be resized so that the pressure on the projected surface of the skirt due to the lateral force of the connecting rod does not exceed 0.5 MPa [31]. The length and angle of the skirt are therefore resized (as shown in the Table 6) using Equation 15. The transverse force in the column "Adapted path 1" is in parentheses because it will have to be redefined from the new geometry of the piston.

	Path 1	Adapted path 1
Skirt length L_s (mm)	40	30
Skirt half angle θ_s (°)	18	30
Projected area on the skirt (mm²)	879	1050
Tranversal load Ft for the case n°5 (N)	494	(494)
Bearing pressure p_s(Mpa)	0,56	(0,47)

Table 6: Piston skirt sizing

Equation 15

$$p_s = \frac{F_t}{D_{piston}.L_s.\sin\left(\frac{\theta_s}{2}\right)}$$

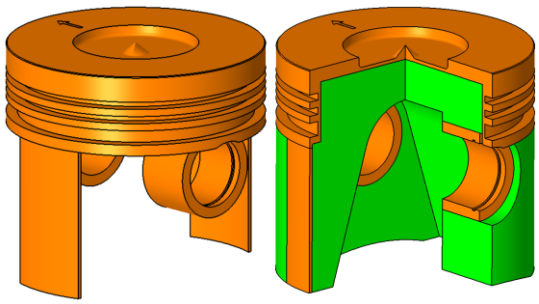

(a)

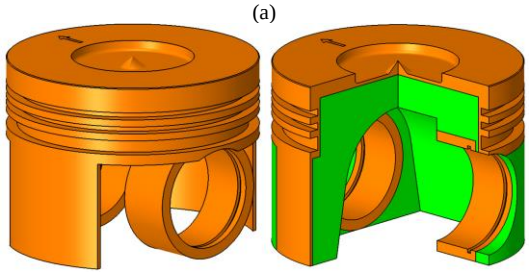

(b)

Fig. 32. (a) Piston from the beginning of the study with the non-design spaces (left), with the design spaces (right); (b) Piston with optimised non-design spaces (left), with design spaces (right). (colour figure online)

The connecting rod and crankshaft have been adapted accordingly, especially the dimensions of the big-end bearing for the first and on the counterweight for the second. CAD is shown at the Fig. 33.

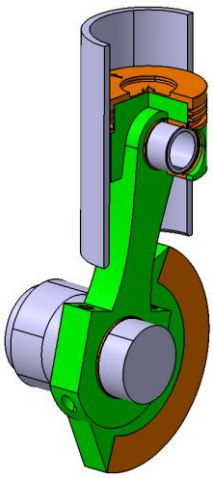

Fig. 33. All parts with design spaces in green and non-design spaces optimised in orange (colour figure online)

3.4.2. Results of second study

The piston then the connecting rod and finally the crankshaft are optimised according to path 1 under the same conditions described above. The results of the different optimisation loops are detailed in Fig. 34 for the piston and on Fig. 35 for the connecting rod.

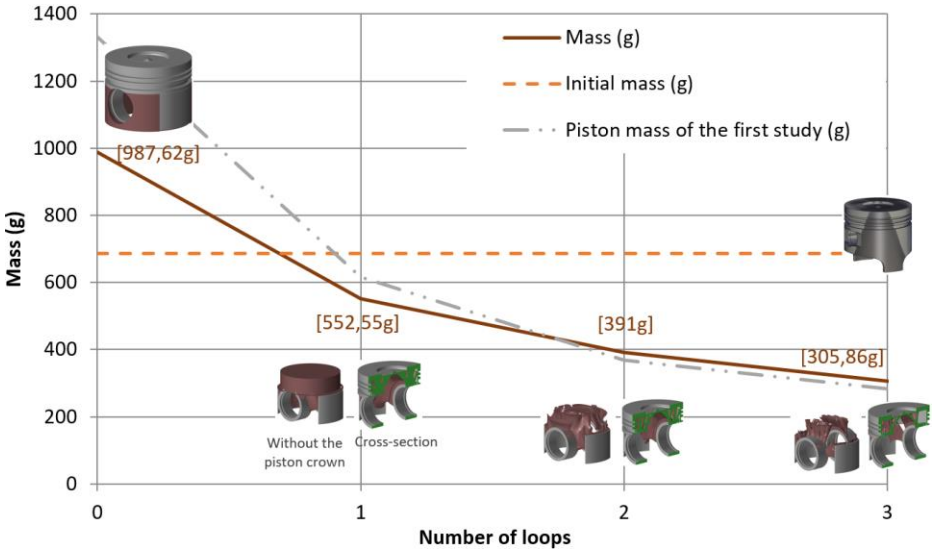

Fig. 34. Evolution of piston mass during optimisations (colour figure online)

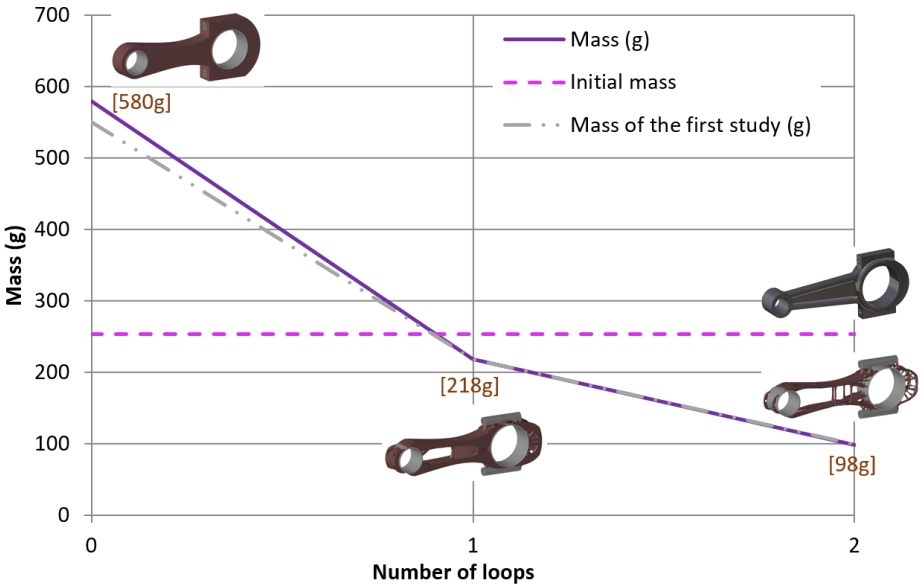

Fig. 35. Evolution of the mass of the connecting rod during optimisations (colour figure online)

A finite element study validates the resistance of the piston and connecting rod as shown in the Fig. 36. The boundaries conditions are the same as the optimization (as shown in Fig. 12). Load cases are those of the Fig. 7 for the piston, and the Fig. 8 for the connecting rod.

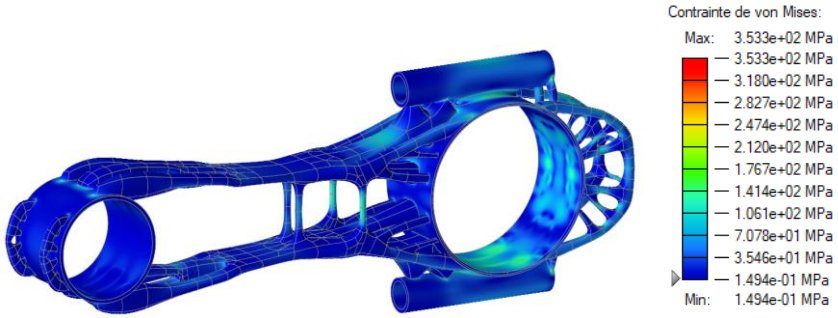

Fig. 36. Optimised connecting rod finite element analysis (colour figure online)

Finite element analysis indicates that the maximum Von Mises stress is 353.3MPa, so the safety coefficient is 2.34.
Vibration analysis (Fig. 37) shows that the bouncing and longitudinal vibrations is docked-identical to study 1. The gains are therefore similar.

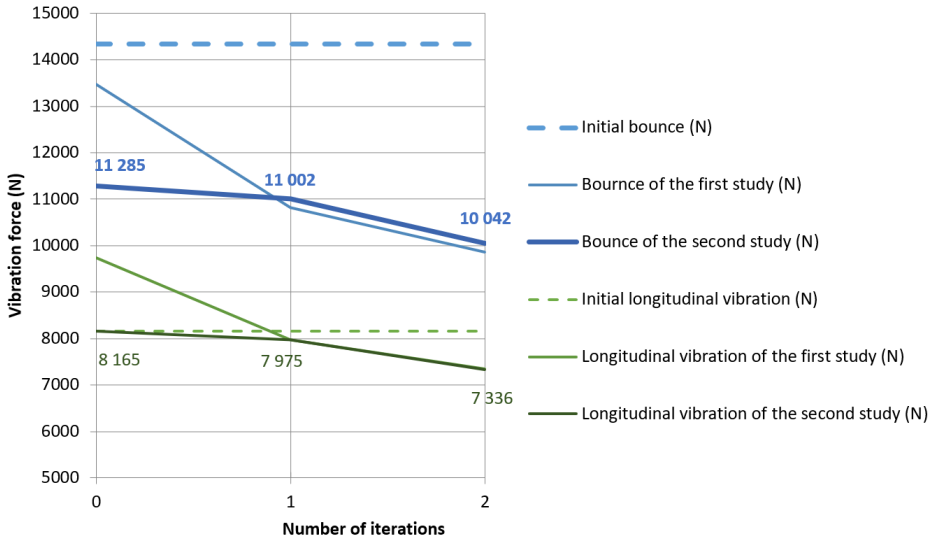

Fig. 37. Evolution of the bouncing and longitudinal vibrations during optimisations (colour figure online)

Table 7 shows the results and gains for each of the two studies (for the redesigned parts).

	Piston			Connecting Rod		
	Original	First study	Second study	Original	First study	second study
Picture	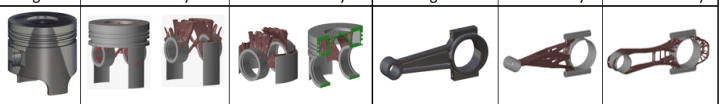					
mass (g)	687	317	340	253	100	98
Gain (%)		54	51		61	61
Bounce (N)	14335	11098	10883	14335	9868	10329
Gain (%)		23	24		31	28
Longitudinal vibration (N)	8165	8165	8165	8165	7345	7336
Gain (%)					10	10
coeff of security	2,2	1,76	1,8	3	2	2,34

Table 7: Table summarizing the results of the two studies

3.4.3. Discussion

The results of the second study show a mass gain of the assembly {Piston; connecting rod; crankshaft} of 27% compared to the original engine. This reduces bouncing vibration forces by 30% and longitudinal vibration by 10%.

Both studies have comparable gains in terms of mass (equal to 26%) and impact on mechanical behaviour. Study 2 also shows a holding of the parts guaranteeing a better service life (safety coefficient higher than study 1 and eigen frequency).

Thus this study demonstrates the interest of taking into account the impact of topological optimisations on interconnection surfaces.

4. Conclusion

In conclusion, it has been shown that for a complex system the TOMS method can bring a gain on mechanical performance. The additional mass gain (following the optimisation loops) also makes it possible to lighten the mechanism, which implies a reduction in material cost as well as consumption.
Furthermore, the study of non-design spaces demonstrates the importance of involving them during optimisation cycles. On the one hand, it is shown that during optimisation, the stress values could change and the original dimensions may not respond efficiently to the performance requirements. On the other hand, it is shown that by redesigning these spaces, it is possible to improve the mechanical strength of the parts as well as their service life.
In perspective, in order to carry out an optimisation of the design space in parallel with the non-design space, a mathematical tool will have to be developed. This tool will be able to perform a topological optimisation (for the DS) in parallel with a parametric optimisation (for the NDS). Thus, the topological optimisation will provide a concept that meets an objective and constraints, while the parametric optimisation will adapt the parameters of the NDS to match the results of the topological optimisation.

5. Bibliography

[1] A. Paolini, S. Kollmannsberger, E. Rank, Additive manufacturing in construction: A review on processes, applications, and digital planning methods, Addit. Manuf. 30 (2019) 100894. https://doi.org/10.1016/j.addma.2019.100894.

[2] J. Gray, C. Depcik, Review of additive manufacturing for internal combustion engine components, SAE Int. J. Engines. 13 (2020) 617–632. https://doi.org/10.4271/03-13-05-0039.

[3] P. Nyamekye, S. Golroudbary, H. Piili, P. Luukka, A. Kraslawski, Impact of additive manufacturing on titanium supply chain : Case of titanium alloys in automotive and aerospace industries, Adv. Ind. Manuf. Eng. 6 (2023) 100112. https://doi.org/10.1016/j.aime.2023.100112.

[4] J.C. Najmon, S. Raeisi, A. Tovar, Review of additive manufacturing technologies and applications in the aerospace industry, in: F. Froes, R. Boyer (Eds.), Addit. Manuf. Aerosp. Ind., Elsevier, 2019: pp. 7–31. https://doi.org/10.1016/B978-0-12-814062-8.00002-9.

[5] B. Blakey-Milner, P. Gradl, G. Snedden, M. Brooks, J. Pitot, E. Lopez, M. Leary, F. Berto, A. du Plessis, Metal additive manufacturing in aerospace: A review, Mater. Des. 209 (2021) 110008. https://doi.org/10.1016/j.matdes.2021.110008.

[6] M. Armstrong, H. Mehrabi, N. Naveed, An overview of modern metal additive manufacturing technology, J. Manuf. Process. 84 (2022) 1001–1029. https://doi.org/10.1016/j.jmapro.2022.10.060.

[7] T.P. Ribeiro, L.F.A. Bernardo, J.M.A. Andrade, Topology optimisation in structural steel design for additive manufacturing, Appl. Sci. 11 (2021) 2112. https://doi.org/10.3390/app11052112.

[8] J. Zhu, H. Zhou, C. Wang, L. Zhou, S. Yuan, W. Zhang, A review of topology optimization for additive manufacturing: Status and challenges, Chinese J. Aeronaut. 34 (2021) 91–110. https://doi.org/10.1016/j.cja.2020.09.020.

[9] M. Orquéra, S. Campocasso, D. Millet, Some principles to optimise an additively manufactured multi-component product, J. Eng. Des. 31 (2020) 219–240. https://doi.org/10.1080/09544828.2019.1699034.

[10] M.K. Thompson, G. Moroni, T. Vaneker, G. Fadel, R.I. Campbell, I. Gibson, A. Bernard, J. Schulz, P. Graf, B. Ahuja, F. Martina, Design for additive manufacturing: trends, opportunities, considerations, and constraints, CIRP Ann. - Manuf. Technol. 65 (2016) 737–760. https://doi.org/10.1016/j.cirp.2016.05.004.

[11] M. Kumke, H. Watschke, T. Vietor, A new methodological framework for design for additive manufacturing, Virtual Phys. Prototyp. 11 (2016) 3–19. https://doi.org/10.1080/17452759.2016.1139377.

[12] P. Pradel, Z. Zhu, R. Bibb, J. Moultrie, A framework for mapping design for additive manufacturing knowledge for industrial and product design, J. Eng. Des. 29 (2018) 291–326. https://doi.org/10.1080/09544828.2018.1483011.

[13] M. Orquéra, Conception pour la fabrication additive : Approche méthodologique pour les systèmes mécaniques multi-corps, PhD thesis, University of Toulon, 2019.

[14] Y. Rong, Z.L. Zhao, X.Q. Feng, Y.M. Xie, Structural topology optimization with an adaptive design domain, Comput. Methods Appl. Mech. Eng. 389 (2022) 114382. https://doi.org/10.1016/j.cma.2021.114382.

[15] H. Rodrigue, M. Rivette, An assembly-level design for additive manufacturing methodology, IDMME - Virtual Concept. (2010) 1–9. https://doi.org/10.1007/978-2-8178-0169-8.

[16] Y. Tang, Y.F. Zhao, Design method for lattice-skin structure fabricated by additive manufacturing, in: ASME. ASME Int. Mech. Eng. Congr. Expo., Montreal, Quebec, Canada, 2014: p. V02BT02A030. https://doi.org/10.1115/IMECE2014-38645.

[17] M. Goelke, 5 ways to rethink optimization, (2016). https://altairuniversity.com/24623-5-ways-to-rethink-optimization/ (accessed December 6, 2017).

[18] O. Diegel, J. Schutte, A. Ferreira, Y.L. Chan, Design for additive manufacturing

process for a lightweight hydraulic manifold, Addit. Manuf. 36 (2020) 101446. https://doi.org/10.1016/j.addma.2020.101446.

[19] L. Rakotondrainibe, G. Allaire, P. Orval, L. Rakotondrainibe, G. Allaire, P. Orval, Topology optimization of connections in mechanical systems, Struct. Multidiscip. Optim. Springer V (2020) hal-02433242.

[20] T. Briard, F. Segonds, N. Zamariola, G-DfAM: a methodological proposal of generative design for additive manufacturing in the automotive industry, Int. J. Interact. Des. Manuf. 14 (2020) 875–886. https://doi.org/10.1007/s12008-020-00669-6.

[21] E. Baron, J.-L. Ligier, Acyclisme des moteurs thermiques - Forces, couples et moments appliqués au moteur monocylindre, Tech. l'ingénieurs. 33 (2017) BM2588 V1.

[22] Erpro group, Material Data Sheet : 316 L, (2019). https://erpro-group.com/wp-content/uploads/2019/04/Fe_316L.pdf (accessed July 1, 2022).

[23] R. Kumar, M. Kumar, J.S. Chohan, Material-specific properties and applications of additive manufacturing techniques: a comprehensive review, Bull. Mater. Sci. 44 (2021) 1–19. https://doi.org/10.1007/s12034-021-02364-y.

[24] M. Orquéra, S. Campocasso, D. Millet, Topological Optimization of a Mechanical System with Adaptive Convergence Criterion, in: Int. Jt. Conf. Mech. Des. Eng. Adv. Manuf., Springer, Cham, 2021: pp. 86–91. https://doi.org/10.1007/978-3-030-70566-4_15.

[25] T. Ramachandran, K.P. Padmanaban, Review on Internal Combustion Engine Vibrations and Mountings, Int. J. Eng. Sci. Emerg. Technol. 3 (2012) 2231–6604.

[26] N.S. Ahirrao, S.P. Bhosle, D. V. Nehete, Dynamics and Vibration Measurements in Engines, in: Procedia Manuf., Elsevier B.V., 2018: pp. 434–439. https://doi.org/10.1016/j.promfg.2018.02.063.

[27] S. Ren, S. Galjaard, Topology optimisation for steel structural design with additive manufacturing, in: Model. Behav. Des. Model. Symp., Springer International Publishing, 2015: pp. 35–44.

[28] J. Kranz, D. Herzog, C. Emmelmann, Design guidelines for laser additive manufacturing of lightweight structures in TiAl6V4, J. Laser Appl. 27 (2015) S14001. https://doi.org/10.2351/1.4885235.

[29] D. Petit, D. Maillet, Techniques inverses et estimation de paramètres. Partie 1, Tech. l'ingénieur Phys. Stat. Mathématique. 42619210 (2008) 1–18.

[30] C. Clos, Technologie des moteurs alternatifs à combustion interne, Tech. l'ingénieur. B2800 (1996) B2800-1.

[31] R. Brun, F. Gastinne, Moteurs thermiques alternatifs, Parties mobiles Pistons et segments, Tech. l'ingénieur. 3 (1983) B396.